

DTMRI Segmentation using DT-Snakes and DT-Livewire

Ghassan Hamarneh and Judith Hradsky

Medical Image Analysis Lab, School of Computing Science, Simon Fraser University
Burnaby, BC, V5A 1S6, Canada

Abstract—In this paper we extend two popular classical scalar medical image segmentation techniques to diffusion tensor magnetic resonance images (DTMRI). We propose DT-snakes and DT-livewire through modifying the external image forces in snakes and cost terms in livewire. The new forces and cost terms are derived from and operate on a DT field rather than a scalar image. This is achieved by making use of recent advances in DT calculus and DT dissimilarity measures, as well as DT smoothing and DT interpolation. Proper quantification of tensor dissimilarity allows for defining spatial gradient vectors and gradient magnitudes of DT fields, an essential component for attracting snakes or livewire to target boundaries in DT images. DT calculus enables weighted averaging of tensors which is essential for both pre-smoothing of DT images prior to segmentation, as well as interpolation of tensors on non-grid positions in the image. We evaluate different recent DT tensor dissimilarity metrics including the Log-Euclidean and the square root of the J-divergence. We present qualitative and quantitative DT segmentation results on both synthetic and real cardiac and brain DTMRI data.

I. INTRODUCTION

Diffusion is the process by which molecules are transported from one part of a medium to another. The flux of diffusing molecules is a result of their random Brownian motion in concentration gradients and is described by Fick's law. Diffusion tensor magnetic resonance imaging (DTMRI) records the diffusion characteristics of water molecules along fiber tracts in-vivo and is becoming increasingly valuable for assessing the effects of disease progression and treatment evaluation on fiber connectivity and diffusion properties [1], [2]. In DTMRI, typically each voxel of the 3D image is assigned a rank three, second order diffusion tensor forming a 3D tensor field. Each tensor is expressed as a 3×3 symmetric, positive semi-definite (PSD) matrix (with nonnegative eigenvalues). The general classes of medical image analysis algorithms performed on scalar medical images (filtering, segmentation, registration and visualization of X-ray CT, T1-weighted MRI, ultrasound, and others) need to be extended to DTMRI tensor fields in order to glean quantitative and qualitative information, potentially improving computer aided diagnosis, follow up of treatment and disease progression, and statistical analysis of structural and functional variability. In the following paragraphs we review important contributions in processing, segmentation, and registration of tensor field data.

The primary goal of processing is to reduce the noise in the DTMRI data that occurs due to various imaging acquisition artifacts. There exist numerous techniques for image processing of scalar fields; an essential task in any image processing pipelines. However, only a few methods have been recently extended to perform basic processing and reduce noise in

diffusion tensor image data, for example median filtering, morphological operations, interpolation, and anisotropic edge preserving smoothing [3], [4], [5], [6].

Identifying and delineating regions of interest (ROI) in image data is necessary for performing subsequent quantitative analysis and qualitative visualization. Segmentation methods rely on (a) identifying nearby voxels with similar diffusion properties and grouping them into one coherent structure, (b) identifying edges in the DTMRI and linking them to form separating boundaries between neighboring structures, and (c) incorporating prior knowledge about the shape characteristics of the different target structures to segment. These intuitive ideas are very well understood for the scalar case, but have only recently been the focus of research for tensor fields [7], [8], [9], [10], [11], [12], [13], [14], [15], [16].

To facilitate viewing and interrogating DTMRI segmentation and visualization results within the context of other medical imaging modalities (e.g. structural MRI), the data sets must be properly fused by bringing them into proper spatial alignment. Image registration is also needed for quantitative and qualitative longitudinal analysis tasks, in which DTMRI data of the same subject at different times must be compared [17], [18], [19], [20].

In this paper we focus on extending two classical and popular scalar image segmentation techniques allowing us to delineate anatomical regions and boundaries directly from DTMRI fields. We utilize the full information in the tensors without being forced to operate on a single derived scalar image such as apparent diffusion coefficient (ADC) or relative anisotropy (RA) [2].

Specifically, we extend snakes [21] and livewires [22] to DT-snakes and DT-livewire primarily by redefining the external image forces and cost terms in snakes and livewire, respectively. The new forces and cost terms now operate directly in the DT field rather than scalar images. This extension relies on recent definitions of tensor dissimilarity metrics, weighted tensor averaging, smoothing and interpolation of DT fields [8], [23], [24]. Since the snakes and livewire methods are formulated such that their contours are attracted to boundaries, the definition of target boundaries is revisited for DTMRI data making use of tensor dissimilarity measures to calculate tensor gradients. We evaluate different alternative DT dissimilarity metrics including the Log-Euclidean and the square root of the J-divergence [23], [8]. Further, because it is known that gradient calculation is sensitive to noise, and in order to avoid having contours attracted to noisy data, the image data is pre-smoothed prior to segmentation, utilizing a DT edge-preserving smoothing algorithm (bilateral DT filtering) [24].

Furthermore, to continue to have deformable models with subpixel accuracy, tensor values need to be evaluated at non-grid positions requiring specialized DT interpolation methods.

The remainder of the paper is organized as follows. In section II we summarize alternative ways of quantifying diffusion tensor dissimilarity and how it is used for tensor gradient calculation. We follow with a summary of the approach we adopt for tensor smoothing and interpolation, and then utilize the previous concepts to propose the extension of snakes and livewire to operate on DT data directly without the need to extract scalar features. In section III we present qualitative experimental and quantitative validation results on synthetic and real brain and cardiac DTMRI data. We summarize and draw conclusions in section IV.

II. METHODS

A. Diffusion Tensor Dissimilarity and Gradient Estimation

Tensors in DTMRI are 3×3 PSD matrices that do not form a vector space thus requiring special attention when performing DT calculations [25]. To perform segmentation we need a way to measure differences between tensors as this will allow us to define gradient vectors that are essential for DT-snakes and DT-livewire, and other potential boundary based DT segmentation techniques. Ideally, tensor dissimilarity should reflect the geodesic distance on the space of allowable tensors; a convex half-cone [26], [25]. Therefore, choosing Euclidean $\|T_1 - T_2\|$, or Frobenius norm $\|T_1 - T_2\|_F$, where $\|A\|_F = \sqrt{\text{Tr}(AA^H)}$ and $\text{Tr}(\dots)$ denotes trace, is not appropriate for measuring distances between tensors T_1 and T_2 . The following are the two main alternatives tensor distance measures recently introduced in the literature which we will utilize to define DT gradients. The Log-Euclidean distance and the affine-invariant square root of the J-divergence [8], denoted respectively as $d_{T_{LE}}$ and d_{T_J} , are given by

$$d_{T_{LE}}(T_1, T_2) = \|\log(T_1) - \log(T_2)\| \quad (1)$$

$$d_{T_J}(T_1, T_2) = \frac{1}{2} \sqrt{\text{Tr}(T_1^{-1}T_2 + T_2^{-1}T_1) - 2n} \quad (2)$$

where \log denotes matrix logarithm, and $n = 3$ for three dimensional diffusion.

The tensor field gradient can now be defined in a manner analogous to central finite difference approximation of the scalar 2D image gradient $\nabla f(x, y)$,

$$\nabla f(x, y) = \frac{1}{2} \begin{bmatrix} f(x+1, y) - f(x-1, y) \\ f(x, y+1) - f(x, y-1) \end{bmatrix}. \quad (3)$$

We replace the finite difference (subtraction) approximation with central tensor dissimilarity to obtain the tensor gradient vector ∇T at any location (x, y) as follows,

$$\nabla T(x, y) = \frac{1}{2} \begin{bmatrix} d_T((T(x+1, y), T(x-1, y))) \\ d_T((T(x, y+1), T(x, y-1))) \end{bmatrix} \quad (4)$$

where d_T is either one of the tensor distance measures presented earlier (equation (1) or (2)).

B. Diffusion Tensor Smoothing

To produce stable gradient calculation and to avoid having contours attracted to noisy data, the image data is typically pre-smoothed prior to segmentation. We utilize a recently proposed bilateral edge-preserving DT field smoothing [24] that relies on calculating a weighted average of tensors using

$$T(x) = k(x)^{-1} \exp \left(\sum_{i=1}^N w_i(x) \log(T(\xi_i)) \right) \quad (5)$$

$$k(x) = \sum_{i=1}^N w_i(x) \quad (6)$$

where \exp is the matrix logarithm, $T(x)$ is the tensor resulting from a weighted averaging of N tensors, $T(\xi_i)$, in the neighbourhood of x . The corresponding weights, w_i , are defined to be inversely proportional to the spatial distance and the tensor dissimilarity between the neighboring tensors and the center tensor, as follows

$$w_i(x) = \alpha f_1(d_T(T(x), T(\xi_i))) + (1 - \alpha) f_2(d_S(x, \xi_i)) \quad (7)$$

where $\alpha \in [0, 1]$ controls the relative emphasis on spatial versus tensor distance, $d_T(T(x), T(\xi_i))$ and $d_S(x, \xi_i)$ are the tensor dissimilarity and spatial distance between $T(x)$ and $T(\xi_i)$, respectively, and f_1 and f_2 are monotonically decreasing functions that map the range of tensor-dissimilarity values and spatial distances, respectively, to the interval $[0, 1]$.

C. Diffusion Tensor Interpolation

To extend the classical deformable models with subpixel accuracy, tensor values need to be evaluated at non-grid positions, requiring specialized DT interpolation methods. As described in [24], DT field interpolation is treated as a special case of (5). A tensor is interpolated at any non-grid position using the Log-Euclidean weighted sum of N nearby tensors, $T(\xi)$, where the weights are inversely proportional to the spatial distance between the non-grid position x and the locations of the nearby tensors, ξ . This is intuitively and conveniently obtained by setting $\alpha = 0$ in equation (7).

Based on the ideas put forward thus far, in the following sections we extend two classical segmentation methods, namely snakes and livewire [21], [22], to operate on diffusion tensor data.

D. DT-Snakes for DTMRI

Snakes are energy-minimizing parametric contours that deform to segment target structures. We extend snakes to operate on DTMRI data. Our implementation takes the form of a polygonal discrete active contour model [21], where the nodes (vertices) of the snake are updated through the application of internal (tensile and flexural) and external (image and inflation) forces. Internal forces are implemented as in the scalar image case [27], while external forces are modified to operate on DT fields in the following ways. The image force, F_i^{image} , at snake node i , attracts the snake to DT field edges and is redefined as follows (Fig. 1)

$$F_i^{image} = -\nabla \|\nabla T(x_i, y_i)\| \quad (8)$$

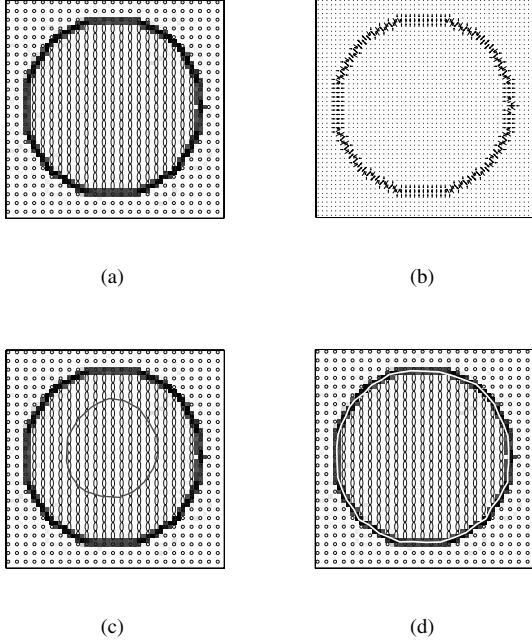


Fig. 1. DT-snake segmentation of a synthetic DT field. The DT image in (a) contains two homogeneous regions with different diffusion properties (a disk and the background). The tensors are visualized using ellipses with major and minor axes proportional to the largest and second largest eigenvalues of the tensor, respectively. A backdrop is displayed as a scalar intensity image with brightness inversely proportional to the tensor gradient magnitude. The DT-snake external force vector field is shown in (b). The initialized DT-snake is shown in (c). After the application of internal, external and inflation forces the DT-snake properly identifies the boundary between the two regions (d).

where ∇T is defined as in (4) and (x_i, y_i) is the location of the snake node i . The inflation force, $F_i^{inflation}$, allow the snake to be initialized farther away from the target boundary [28] and is redefined as follows

$$F_i^{inflation} = \text{sign}(d_T(T(x_i, y_i), T^{ref}) - t)n_i \quad (9)$$

where d_T is defined in equation (1) and(2), T^{ref} is a reference tensor obtained by Log-Euclidean averaging of an ROI within the target structure, n_i is the unit vector in the direction normal to the contour at node i , and t is a tensor distance threshold analogous to the scalar case [29].

E. DT-Livewire for DTMRI

The livewire method relies on the definition of a local cost, $C(p, q)$, between neighboring pixels, p and q , to calculate globally optimal paths delineating boundaries of target structures between interactively-selected seed and target points in the image [22]. In addition to terms that encode path smoothness or shortness constraints in $C(p, q)$, terms that favor paths following high gradient magnitude while minimizing change in gradient direction are encoded as well (vis-à-vis internal and external energy terms in snakes). Internal constraint terms need not be extended to deal with DTMRI data. However, external gradient magnitude and direction are modified as follows. The

gradient magnitude cost term for any pixel q is now redefined as

$$f_M(q) = 1 - \|\nabla T(q)\|/\|\nabla T(q)\|_{max} \quad (10)$$

where $\|\nabla T\|_{max}$ represents the largest DT gradient magnitude in the image and ∇T is as defined in (4), and the gradient direction cost term for connecting pixel p to pixel q is now redefined as

$$f_D(p, q) = \frac{1}{\pi} \arccos \left(\frac{\nabla T(p) \nabla T(q)}{\|\nabla T(p)\| \|\nabla T(q)\|} \right) \quad (11)$$

The reader is referred to [22] for details on the derivations of the scalar versions of equations (10) and (11).

III. EXPERIMENTS AND RESULTS

The DT processing and segmentation tools we develop relate to two long term clinical applications. Firstly, we are investigating the effect of disease progression and treatment in multiple sclerosis patients on inter-hemispheric fibre connectivity and diffusion properties within different regions of the corpus callosum (CC) bridge [30], [31]. Secondly, we are studying the properties of the laminar cardiac fibre sheet in the myocardium from DTMRI. Examples of DT-snakes and DT-livewire on synthetic and real (cardiac and brain) DT image data are provided in this section.

Fig. 1 shows the results of applying DT-snakes to a synthetic DT image example. The image contains two regions; a disk and background. Each region is populated with a homogeneous field of tensors (Fig. 1(a)). The external force vector field resulting from this DT data is shown in Fig. 1(b). A DT-snake is initialized within the disk via mouse-clicks. During initialization, the user has the option of viewing any scalar field derived from the diffusion tensor field (e.g. largest eigenvalue, RA, ADC, or tensor gradient magnitude) or an inherent tensor visualization, or a combination of the two (Fig. 1(c)). The final result (Fig. 1(d)) of DT-snake deformation with internal and external (including inflation) forces shows how the snake latched to the interface between the two regions with different diffusion properties.

In Fig. 2, we demonstrate the effect of smoothing on the performance of DT-livewire segmentation, given the same number and same location of seed points, while changing the amount of noise in the DT image. DT-livewire performs extremely well as expected when no noise is introduced and manages to identify the interface between two homogeneous regions with different diffusion properties. The performance deteriorates when noise is added to the image and improves again after applying bilateral DT filtering to reduce the noise.

In Fig. 3, we segment the corpus callosum from brain DTMRI using DT-snakes. An approximate DT-snake is initialized quickly by the user and then left to deform according internal and external forces. Given the rough initialization, the DT-snake latched to the corpus callosum DT boundary.

In Fig. 4, we segment the endocardium from heart DTMRI using DT-snakes. Given a rough initialization of the DT-snake inside the heart chamber, the DT-snake dynamics are simulated until it converges onto the inner heart wall. The

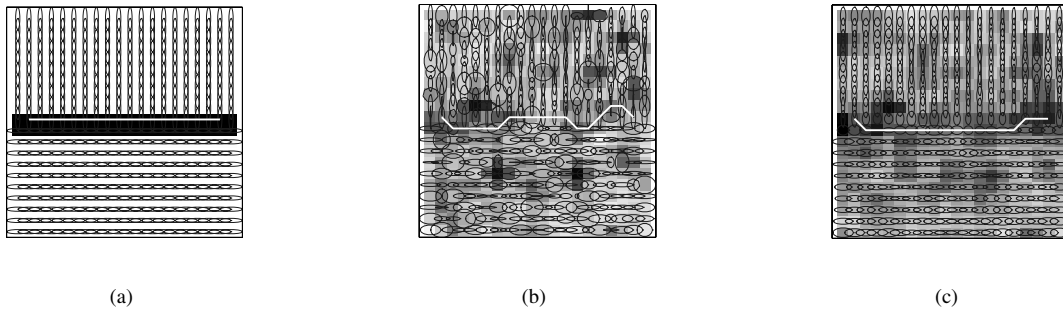


Fig. 2. DT-livewire segmentation and the effect of noise and DT smoothing. In (a-c) a DT-livewire is supplied with the same seed points (terminal points of the white livewire contour). In (a) the DT-livewire is operating on a noise-free synthetic DT field exhibiting two homogeneous regions (top and bottom halves) with different diffusion properties. The livewire successfully latches along the DT interface. In (b), the DT-livewire is operating on a noisy version of (a) and the livewire contour deviates from the correct interface. In (c), the DT field is smoothed (using d_{T_j} , $\alpha = 0.2$, $N = 9$, and 1 iteration) yielding an improved delineation (more similar to the livewire in (a)).

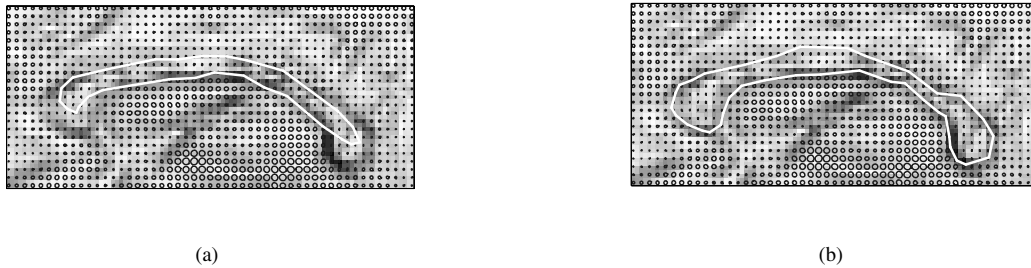


Fig. 3. Segmentation of the corpus callosum from brain DTMRI using DT-snakes. Initial and final snake segmentation are shown in (a) and (b), respectively. The DT-snake contours are plotted in white. The tensors are visualized using ellipses with major and minor axes proportional to the first and second eigenvalues of diffusion tensor, respectively. The backdrop is a scalar intensity image inversely proportional to the tensor gradient magnitude estimated using $d_{T_{LE}}$.

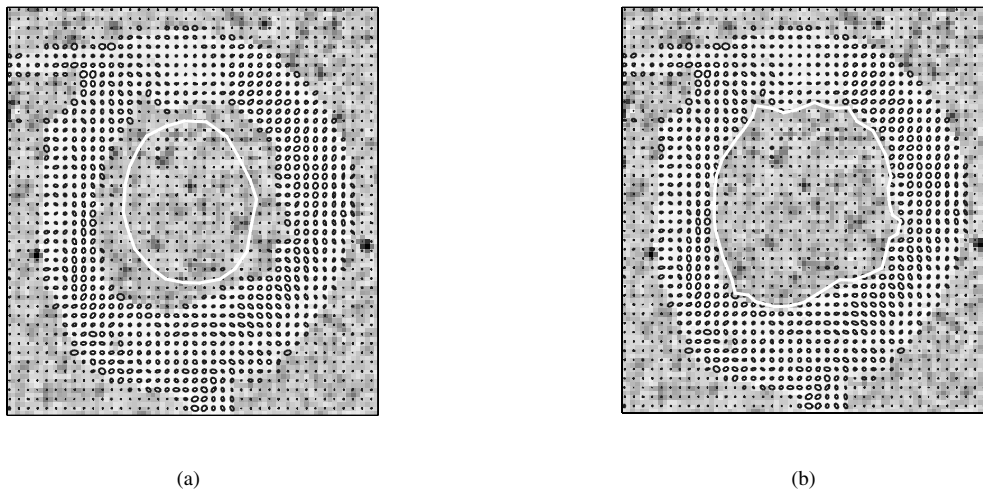


Fig. 4. Segmentation of the endocardium from heart DTMRI using DT-snakes. Initial and final snake contours are plotted in white in (a) and (b), respectively. Tensor field and scalar intensity backdrop are visualized similar to Fig. 3.

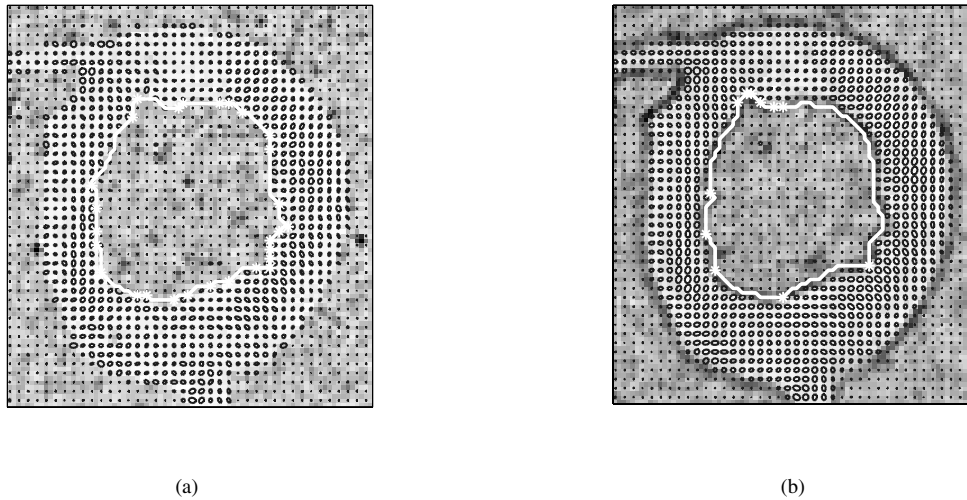


Fig. 5. Segmentation of the endocardium from heart DTMRI using DT-livewire. DT-livewire is applied to (a) the original noisy DTMRI slice and to (b) a smoothed version of the DT data (section II-B). Less number of user-selected seed points are required for performing segmentation when the data is smoothed. The DT-livewire contour is shown in white and seed points are shown as white asterisks. Diffusion tensors and backdrop are visualized as in earlier figures.

use of DT-based inflation force allows the snake contour to be initialized farther away from the heart wall (even in regions with almost no tensor gradient). This behavior has been demonstrated previously for scalar snakes, here the same behavior is observed for DT-snakes.

In Fig. 5, we apply DT-livewire to the segmentation of the endocardium from heart DTMRI. This example demonstrates that livewire now operates on tensor data, as evidenced by the livewire contour latching to inner heart wall between successive seed points. This example also demonstrates bilateral smoothing of DT fields and how it reduces the amount of seed points required to complete the livewire segmentation, compared to the original noisy data.

In Fig. 6, we segment the corpus callosum from brain DTMRI using DT-livewire. As in the previous example, smoothing results are visualized and its effect on DT-livewire segmentation is demonstrated, namely reducing the number of seed points the user needs to manually specify.

IV. CONCLUSION

DTMRI provides unique *in-vivo* measurements of fibre structure in the body. The measurements are presented as 2D or 3D images where each pixel or voxel holds a 3×3 matrix. There is a strong interest in the biomedical image computing community to process, visualize, and analyze this type of data in order to extract clinically relevant information related to diagnosis and therapy of cardiac, neurological, and other pathologies. However, the majority of existing techniques are designed to operate on scalar fields (or RGB images) and more work is needed to provide a diverse set of algorithms and tools at par with what is available for scalar images. In this work we extend two classical and popular 2D scalar image segmentation techniques to operate on DT fields to delineate

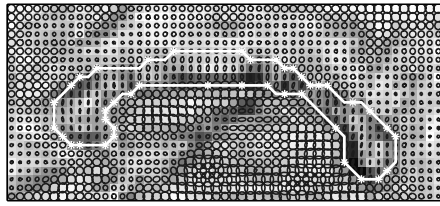
regions of interest according to their anisotropic diffusion and fibre orientation properties. Specifically, we extended snakes and livewire to DT-snakes and DT-livewire by redefining the external image forces and cost terms, through making use of recent advances in DT smoothing, interpolation, and dissimilarity metrics. We demonstrated these extensions through several synthetic and real cardiac and brain DT segmentation examples. We do not attempt to solve the initialization and parameter sensitivity weaknesses of scalar snakes or to avoid the need for interactive seed selection of livewire. These issues are still exhibited in DT-snakes and DT-livewire. Future work includes more rigorous evaluation of the performance of the methods, extending other classical scalar image processing and analysis algorithms to operate on 3D DT fields, and the segmentation of multiple DT images related to specific clinical applications (e.g. multiple sclerosis) and examining relationships between fibre properties in segmented regions and disease progression or treatment evaluation.

ACKNOWLEDGEMENTS

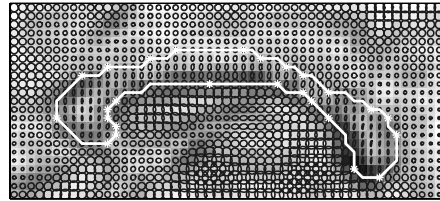
Drs. Patrick A. Helm and Raimond L. Winslow at the Center for Cardiovascular Bioinformatics and Modeling and Dr. Elliot McVeigh at the National Institute of Health for provision of the cardiac DTMRI data. Dr. Khader Hasan, Department of Diagnostic and Interventional Imaging, University of Texas Medical School at Houston, for provision of the brain DTMRI data.

REFERENCES

- [1] E. O. Stejskal and J. E. Tanner, "Spin diffusion measurements: spin echoes in the presence of a time-dependent field gradient," *J. Chem. Phys.*, vol. 42, pp. 288–292, 1965.
- [2] C.-F. Westin, S. E. Maier, H. Mamata, A. Nabavi, F. A. Jolesz, and R. Kikinis, "Processing and visualization of diffusion tensor mri," *Medical Image Analysis*, vol. 6(2), pp. 93–108, 2002.



(a)



(b)

Fig. 6. Segmentation of the corpus callosum from brain DTMRI using DT-livewire. DT-livewire is applied to (a) the original noisy DTMRI slice and to (b) a smoothed version of the DT data. Less number of user-selected seed points are required for performing segmentation when the data is smoothed (Smoothing and legend are as described in Fig. 5).

[3] M. Welk, C. Feddern, B. Burgeth, and J. Weickert, "Median filtering of tensor-valued images," in *Pattern Recognition*, ser. Lecture Notes in Computer Science, B. Michaelis and G. Krell, Eds., vol. 2781. Springer, Berlin, 2003, pp. 17–24.

[4] B. Burgeth, M. Welk, C. Feddern, and J. Weickert, "Morphological operations on matrix-valued images," in *Computer Vision - ECCV 2004*, ser. Lecture Notes in Computer Science, T. Pajdla and J. Matas, Eds. Springer, Berlin, 2004, vol. 3024, pp. 155–167.

[5] C. Castano-Moraga, M. A. Rodrigues-Flrido, L. Alvarez, C.-F. Westin, and J. Ruiz-Alzola, "Anisotropic interpolation of dt-mri data," in *Seventh International Conference on Medical Image Computing and Computer-Assisted Intervention (MICCAI'04)*, Rennes - Saint Malo, France, 2004.

[6] J. Weickert and T. Brox, "Diffusion and regularization of vector- and matrix-valued images," in *Inverse Problems, Image Analysis, and Medical Imaging*, ser. Contemporary Mathematics, AMS, Providence, M. Z. Nashed and O. Scherzer, Eds., vol. 313, 2002, pp. 251–268.

[7] W. E. L. G. L. O'Donnell and C.-F. Westin, "Interface detection in dtmri," in *Seventh International Conference on Medical Image Computing and Computer-Assisted Intervention (MICCAI'04)*, Rennes - Saint Malo, France, 2004.

[8] Z. Wang and B. Vemuri, "An affine invariant tensor dissimilarity measure and its applications to tensor-valued image segmentation," *CVPR*, vol. (1), pp. 228–233, 2004.

[9] A. Brun, H. Knutsson, H. J. Park, M. E. Shenton, and C.-F. Westin, "Clustering fiber tracts using normalized cuts," in *Seventh International Conference on Medical Image Computing and Computer-Assisted Intervention (MICCAI'04)*, 2004, pp. 368–375.

[10] J. W. C. Feddern and B. Burgeth, "Level-set methods for tensor-valued images," in *Proc. Second IEEE Workshop on Variational, Geometric and Level Set Methods in Computer Vision*, O. Faugeras and N. Paragios, Eds., Nice, France.

[11] R. D. C. Lenglet and O. Faugeras, "Inferring white matter geometry from diffusion tensor mri: Application to connectivity mapping," in *ECCV*, vol. (4), 2004, pp. 127–140.

[12] M. R. C. Lenglet and R. Deriche, "Segmentation of 3d probability density fields by surface evolution: Application to diffusion mri," in

MICCAI, vol. (1), 2004, pp. 18–25.

[13] C. Lenglet, M. Rousson, R. Deriche, O. Faugeras, S. Lehericy, and K. Ugurbil, "A riemannian approach to diffusion tensor images segmentation," in *IPMI*, 2005, pp. 591–602.

[14] C. L. M. Rousson and R. Deriche, "Level set and region based surface propagation for diffusion tensor mri segmentation," in *ECCV Workshops CVAMIA and MMBIA*, 2004, pp. 123–134.

[15] D. T. R. Deriche and C. Lenglet, "Dt-mri estimation, regularization and fiber tractography," in *ISBI 2004*, 2004, pp. 9–12.

[16] M. Wiegell, D. Tuch, H. Larson, and V. Wedeen, "Automatic segmentation of thalamic nuclei from diffusion tensor magnetic resonance imaging," *NeuroImage*, vol. 19, pp. 391–402, 2003.

[17] P. B. D. Alexander, C. Pierpaoli, and J. Gee, "Spatial transformations of diffusion tensor magnetic resonance images," *IEEE Trans. Med. Imag.*, vol. 20, pp. 1131–1139, Nov. 2001.

[18] J. Ruiz-Alzola, C.-F. Westin, S. K. Warfield, C. Alberola, S. E. Maier, and R. Kikinis, "Nonrigid registration of 3d tensor medical data," *Medical Image Analysis*, vol. 6, pp. 143–161, 2002.

[19] A. Guimond, C. R. G. Guttman, S. K. Warfield, and C.-F. Westin, "Deformable registration of dt-mri data based on transformation invariant tensor characteristics," in *ISBI*, Washington (DC), USA, 2002.

[20] I. F. Talos, L. O'Donnell, C.-F. Westin, S. K. Warfield, W. M. Wells, S. S. Yoo, L. Panych, A. Golby, H. Mamata, S. E. Maier, P. Ratiu, C. G. Guttman, P. M. L. Black, F. A. Jolesz, and R. Kikinis, "Diffusion tensor and functional mri fusion with anatomical mri for image guided neurosurgery," in *Sixth International Conference on Medical Image Computing and Computer-Assisted Intervention (MICCAI'03)*, Montreal, Canada, 2003.

[21] A. W. M. Kass and D. Terzopoulos, "Snakes: Active contour models," *International Journal of Computer Vision*, vol. 1(4), pp. 321–331, 1987.

[22] W. A. Barrett and E. N. Mortensen, "Interactive live-wire boundary extraction," *Medical Image Analysis*, vol. 1(4), pp. 331–341, 1996.

[23] X. P. V. Arsigny, P. Fillard and N. Ayache, "Fast and simple calculus on tensors in the log-euclidean framework," in *Proceedings of MICCAI'05*, ser. Lecture Notes in Computer Science, J. Duncan and G. Gerig, Eds. Palm Springs, California: Springer Verlag, Oct. 2005, to Appear.

[24] G. Hamarneh and J. Hradsky, "Bilateral filtering of diffusion tensor mr images," *IEEE Symposium on Signal Processing and Information Technology, ISSPIT 2006*, 2006.

[25] P. F. Xavier Pennec and N. Ayache, "A riemannian framework for tensor computing," *International Journal of Computer Vision*, vol. 65(1), Oct. 2005, note: To appear. Also as INRIA Research Report 5255.

[26] S. J. P.T. Fletcher, "Principal geodesic analysis on symmetric spaces: Statistics of diffusion tensors," ser. Lecture Notes in Computer Science, vol. 3117. Springer-Verlag, 2004, pp. 87–98.

[27] S. Lobrege and M. Viergever, "A discrete dynamic contour model," *IEEE Trans. Med. Imag.*, vol. 14(1), pp. 12–24, 1995.

[28] L. Cohen, "On active contour models and balloons," *CVGIP*, vol. 53, no. 2, pp. 211–218, March 1991.

[29] T. McInerney and D. Terzopoulos, "T-snakes: Topology adaptive snakes," *Medical Image Analysis*, vol. 4, pp. 73–91, 2000.

[30] S. F. Witelson, "Hand and sex differences in the isthmus and genu of the human corpus callosum: A postmortem morphological study," *Brain*, vol. 112, pp. 799–835, 1989.

[31] H. KM, R. Gupta, R. Santos, J. Wolinsky, and P. Narayana, "Fractional diffusion tensor anisotropy of the seven segments of the normal-appearing white matter of the corpus callosum in healthy adults and relapsing remitting multiple sclerosis," *Journal of Magnetic Resonance Imaging*, vol. 21(6), pp. 735–743, 2005.